PERGAMON

Journal of Structural Geology 23 (2001) 819–834

JOURNAL OF STRUCTURAL GEOLOGY

www.elsevier.nl/locate/jstrugeo

Deformation partitioning during folding of banded iron formation

J. Hippertt[a,*], C. Lana[a], T. Takeshita[b]

[a]*Departamento de Geologia, Universidade Federal de Ouro Preto, 35400-000, Ouro Preto, MG, Brazil*
[b]*Department of Earth and Planetary Systems Science, Hiroshima University, Higashi-Hiroshima, 739, Japan*

Received 5 July 1999; accepted 21 June 2000

Abstract

Domainal electron and optical microscopy and *c*-axis fabric analysis are utilized to document microstructures and the associated deformation partitioning between crystal plastic, brittle and fluid-assisted deformation mechanisms during folding of Proterozoic banded iron formation (a hematite–quartz–calcite multilayer) from the Quadrilátero Ferrífero granite–greenstone terrain (southeastern Brazil). The operation of different mechanisms was partially determined by the contrasting rheologic response of these three minerals at greenschist facies metamorphic conditions. Fracturing was the main deformation process in hematite, while solution-transfer accounted for part of the deformation in both calcite and quartz. Notably, there is strong interaction among the different deformation mechanisms, which have influenced each other in various ways. Fracturing of hematite in hinge zones of folds caused opening of gaps, which were sealed by direct precipitation of silica from the fluid phase. As a consequence, a chemical potential gradient between crystals and fluid phase was produced, and quartz was dissolved to restore the thermodynamical crystal–fluid equilibrium. Thus, brittle deformation of hematite partially controlled solution-precipitation creep in quartz. Heterogeneous access of fluid into the deforming medium also affected the deformation processes. Inhomogeneous deformation in the quartz–calcite aggregates generated intergranular porosity and increased fluid access, with solution-transfer becoming dominant in these domains. In contrast, the relatively more homogeneous deformation in the pure quartz aggregates served to maintain well-adjusted grain boundaries and reduced fluid access into the intergranular space, such that these domains deformed uniformly by crystal plastic processes, at relatively dry conditions.

1. Introduction

Under greenschist facies metamorphic conditions, deformation of polymineralic rocks generally occurs through operation of a number of competing deformation mechanisms (e.g. Knipe, 1989; Handy, 1990; FitzGerald and Stünitz, 1993) which reflect the rheologic properties of the deforming materials, the pressure-temperature conditions of deformation, the fluid activity and the applied stress field. This deformation partitioning evolves in parallel with changes in microstructures, which accompany progressive deformation (e.g. grain size reduction, appearance of new minerals due to reaction softening, development of crystallographic fabrics, etc.). The specific combination of deformation mechanisms at each given instant of the strain path is expected to reflect the energetically most economic way to accommodate imposed deformations. Detailed microstructural analyses may provide insight into the comparative efficiency of the different deformation mechanisms for each specific microstructure and deformation conditions, as well as to elucidate the evolving deformation partitioning during progressive deformation. Previous work on high strain tectonites such as ultramylonites and phyllonites from different protolith rocks (e.g. Stünitz and FitzGerald, 1993; Hippertt and Hongn, 1998) has shown that these rocks tend to develop a relatively homogeneous stable-state microstructure where only a single or a few deformation mechanisms operate. Hence, by studying the initial stages of deformation in polymineralic rock composed of minerals with contrasting rheologic properties, we expect to identify the first mechanism switches that occur during progress towards this more homogeneous microstructure.

The Proterozoic banded iron formation (BIF) of Quadrilátero Ferrífero region, southeastern Brazil, provides a good natural laboratory to investigate competing deformation mechanisms during multilayer folding in general strain. These layered rocks are composed of three minerals with contrasting rheological properties (hematite, quartz and calcite) and were folded under greenschist facies metamorphic conditions and in the presence of an aqueous fluid phase. They developed a pronounced deformation partitioning between crystal plastic, brittle, and fluid-assisted deformation processes. In this paper, by utilizing domainal optical and electron microscopy and

* Corresponding author.

0191-8141/01/$ - see front matter
PII: S0191-8141(00)00128-0

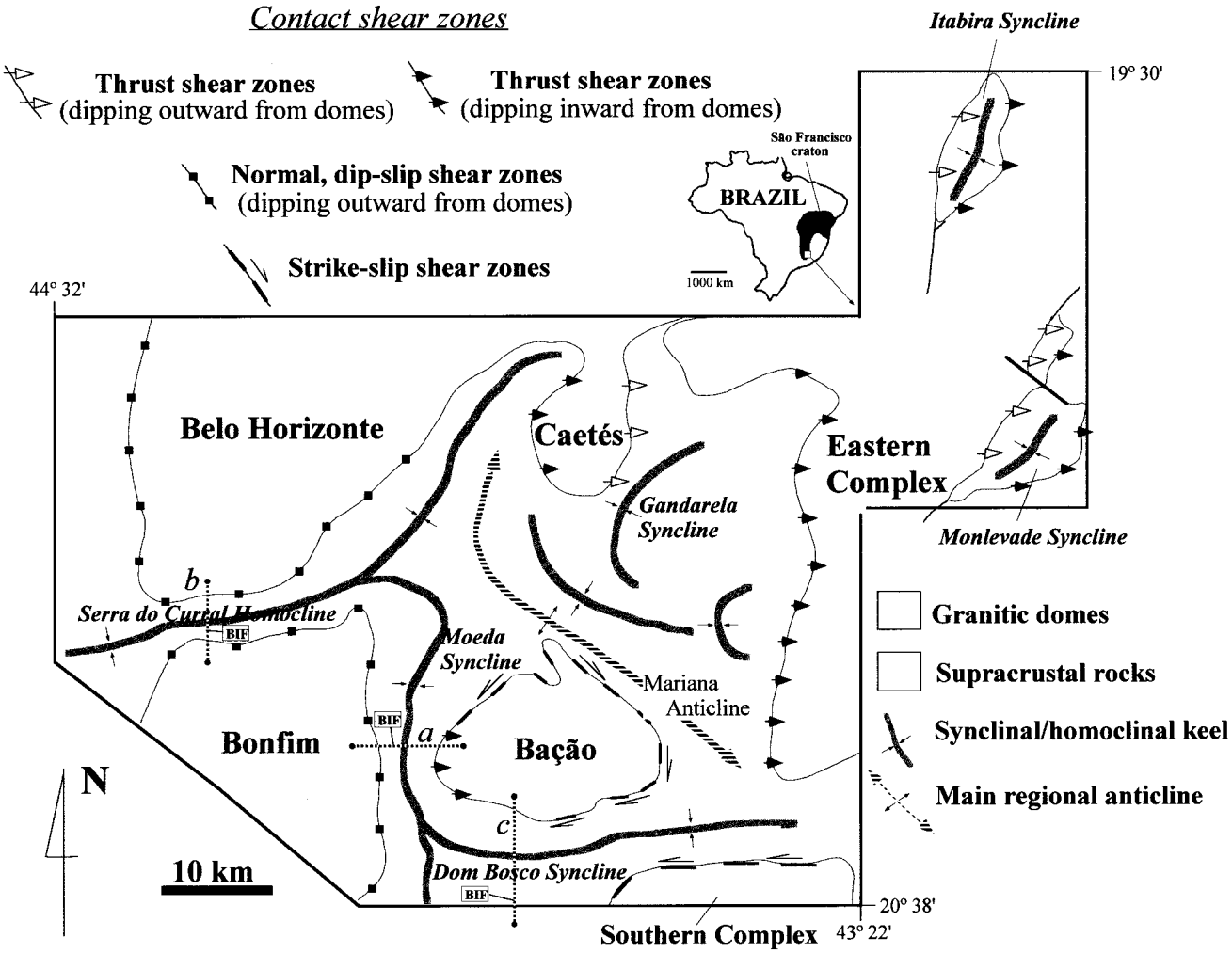

Fig. 1. Simplified geologic-structural map of the Quadrilátero Ferrífero granite-greenstone terrain of southeastern Brazil. The investigated profiles across the folded metasedimentary sequences are indicated by 'a', 'b' and 'c'. Location of the sampled iron banded formation occurrences (BIF) are also indicated.

domainal quartz *c*-axis fabric analyses, we investigate the spatial distribution of and transitions between the different deformation mechanisms, and discuss the physical-chemical factors that control their operation.

2. Geological setting

The Proterozoic BIF of Quadrilátero Ferrífero is a several hundred metres-thick sequence of metasedimentary rocks (Itabira group) whose layered structure is currently attributed to shallow marine precipitation controlled by daily temperature variations (Castro, 1994). They have been regionally metamorphosed to greenschist to lower amphibolite facies (Herz, 1978) during the Transamazonian (2.0–1.7 Gyr) and Pan-African-Brasiliano (1.0–0.6 Gyr) orogenies that affected the Quadrilátero Ferrífero granite greenstone terrain (Marshak et al., 1992) (Fig. 1). Intense folding, foliation development and shear zone development at low metamorphic grade conditions took place during the 1.0–0.6 Gyr Pan-African-Brasiliano orogeny, the most pervasive tectonic event recorded in the BIF and other metasedimentary rocks of the Quadrilátero Ferrífero (cf. Chauvet et al., 1994). This regional metamorphism occurred in the presence of an aqueous fluid phase as indicated by extensive phyllonitization, feldspar breakdown through mica-producing softening reactions, solution-transfer and associated gold mineralization in shear zones (e.g. Chauvet et al., 1994; Hippertt, 1998).

The BIF is intensely folded and kinked from microscopic to regional scale within macroscale synclines which anastomose around the granitic–gneissic domes of the Quadrilátero Ferrífero. This unit can be followed for more than two hundred kilometres within these synclines, always showing a pattern of asymmetric folds and kinks with vergence outward from the granitic domes (Fig. 2). This pattern is a consequence of returning mass flow in the overlaying supracrustals during ascent of the granitic–gneissic domes, which is interpreted as the ultimate driving force for development of the surrounding macroscale synclines and

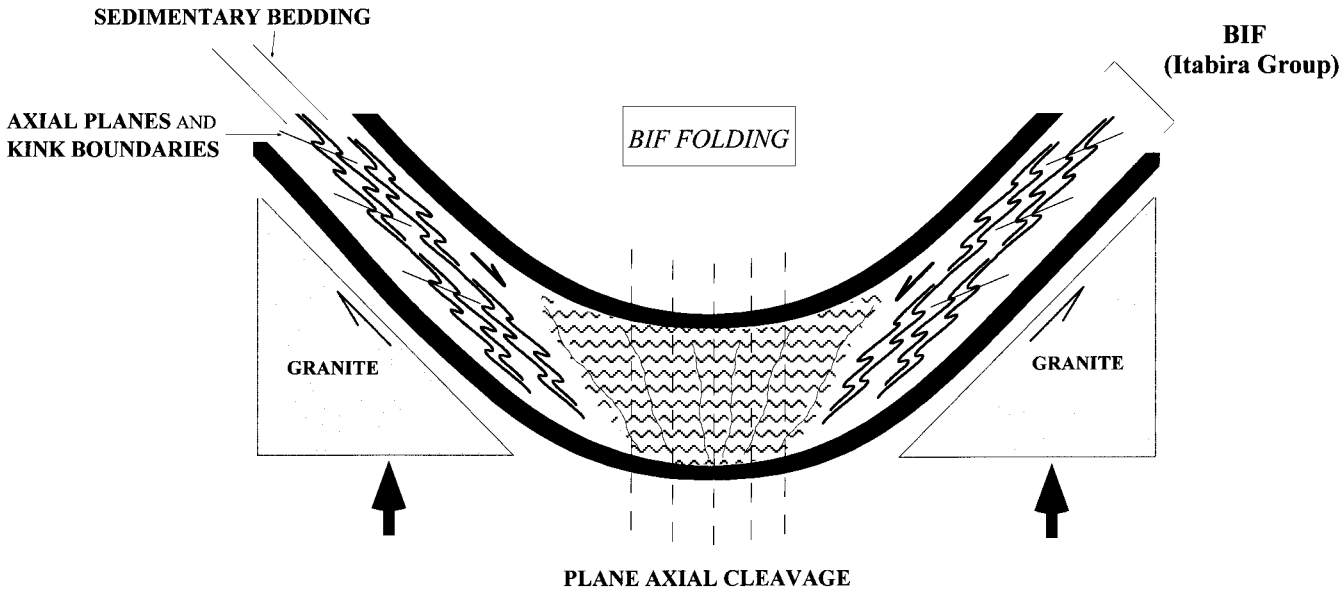

Fig. 2. Idealized sketch illustrating the general pattern of metre to centimetre scale secondary folds and kinks observed in the BIF sequences, which were folded within the regional scale synclines of the Quadrilátero Ferrífero. In the syncline limbs, axial planes of secondary asymmetric folds and kink boundaries dip toward the syncline axis. In the hinge zones, crenulation and plane axial cleavage are predominant. This paper investigates deformation mechanisms in selected decimetre-scale asymmetric folds that follow this regional structural pattern.

associated folding on a wide range of scales (Hippertt and Davis, 2000). Because of the strong rheological contrast between their rock-forming minerals, the BIF has developed much more pronounced folding patterns than the overlaying and underlaying metavolcanic–sedimentary units (Archaean and Proterozoic schists, quartzites and phyllites).

The BIF of Quadrilátero Ferrífero shows three main compositional lithotypes. The Fe oxide-rich type is composed of predominantly hematite and/or magnetite with minor amounts of other minerals. The quartz-rich type is a quartzite containing hematite and/or magnetite in variable proportions. This is the most common lithotype, which is regionally called 'itabirite'. The carbonitic lithotype, focused on in this paper, contains calcite and/or dolomite plus quartz and Fe oxides in variable proportions, and shows more pronounced folding than the other two lithotypes. These lithotypes prograde laterally and vertically one into another throughout the Quadrilátero Ferrífero region. The reader is referred to Chemale et al. (1994) for more details on the geological and structural setting of the Quadrilátero Ferrífero. Oriented samples for this study were collected in three iron mines located in the Moeda syncline, Dom Bosco syncline and Serra do Curral homocline (Fig. 1).

3. Microstructure

3.1. Fold geometry

The rocks sampled for microstructural investigation have folds whose wave length ranges from hundred micrometers to tens of centimetres (Fig. 3). These folds are mostly asymmetric, with well-defined long and short limbs, and show varied inclinations, which are consistent with the predominant vergence outward from the granite domes. In the short limbs of the decimetric folds (herein referred to as 'host folds'); however, millimetre and centimetre-scale folds (referred to as 'secondary folds') may show an opposite vergence and more symmetric morphologies. These secondary folds are commonly associated with quartz veining and fracturing of hematite layers. A new, planar axial foliation is also incipiently developed in the hinge zones of the decimetre scale host folds. As generally occurs during multilayer folding, the tightest secondary folds occur in the thinnest rock layers.

The secondary folds show a wide range of inclination angles which vary along the host fold domains. In the long limbs of the host folds, the secondary folds attain the highest degree of inclination and the vergence is always consistent with that of the asymmetric host fold. Close to the inflection line, some secondary folds are extremely inclined and resemble recumbent folds. Towards the hinge zone, however, the asymmetry of the secondary folds tends to decrease. The short limbs of host folds show secondary folds that are symmetric or display only a subtle opposing asymmetry relative to the host fold.

3.2. Layer types

The BIF shows four main types of alternating layers with distinct composition and microstructure (quartz–calcite, quartz–hematite, quartz-rich, and hematite-rich layers; Fig. 4), which in part correspond to the original sedimentary

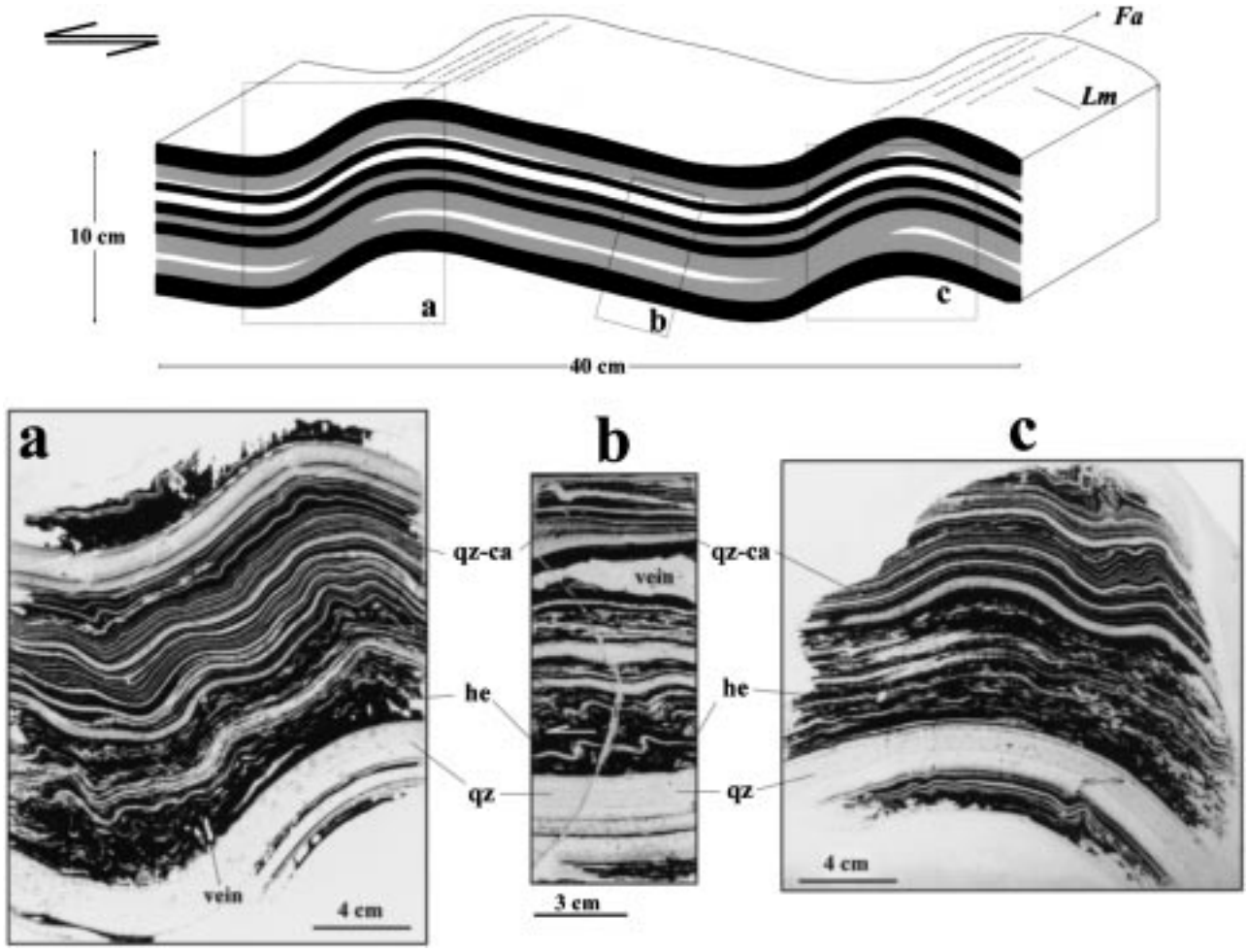

Fig. 3. Views of the short limb (a), long limb (b) and hinge zone (c) of one investigated decimetric fold from the Dom Bosco Syncline, as observed in a section perpendicular to the fold axis. Some quartz-rich (qz), hematite-rich (he) and quartz–calcite layers (qz–ca) are indicated. Note the consistent asymmetry of the millimetre–centimetre scale secondary folds in the long limbs. In contrast, in the short limbs, the secondary folds are more symmetric. Fold axis (Fa) and mineral lineation defined by elongate hematite flakes (Lm) are also indicated.

bedding (Castro, 1994), and in part are of tectonic origin (discussed below). The proportion of these different layers varies greatly. For microstructural purposes, we have selected for investigation samples where the different layers occur with similar proportions, except the quartz–hematite layers, which always occupy a minor volume proportion.

The quartz–calcite layers contain these two minerals in equal proportions, and generally as polygonal and/or slightly curved grains (40–150 μm), with minor amounts of hematite also present. These layers (thickness 1–20 mm) are distinguished from the others by typically showing thinned limbs and thickened hinge zones, and a spatial association with quartz veins. Three-dimensional SEM observation of quartz and carbonate grains from these layers reveals a noticeable intergranular porosity and the presence of irregular, "corroded" grain boundaries (Fig. 5b,c). There are two varieties of quartz–calcite layers (Fig. 4b–d) that reflect the degree of deformation. In the less deformed/folded domains, quartz and calcite grains occur homogeneously disseminated throughout the layers, with a minor part of the carbonate minerals occurring as poikiloblastic calcite porphyroblasts. In the more deformed domains, however, there is a clear separation of these two mineral phases with quartz being segregated as irregular nodules, cutting veins or along planar zones on the layer boundaries (Fig. 4b). This tendency is demonstrated by the statistical clustering analysis made in folded quartz–calcite layers with variable fold closures (interlimb angles between 32° and 125°; Fig. 6), where the degree of clustering increases with the progressive fold closure.

The hematite-rich layers are composed of planar hematite crystals (long dimension 30–200 μm) which are oriented parallel to the folded surface, with minor amounts of quartz occupying gaps between the hematite crystals. These layers keep a constant thickness (varying between 100 μm and 40 mm) through the different fold domains. Thin hematite layers (thickness <150 μm) tend to be disrupted or develop a profusion of tight, micrometer/millimetre scale intrafolial folds. Gaps along the contact with the adjacent layers are commonly developed in the concave side of folded hematite

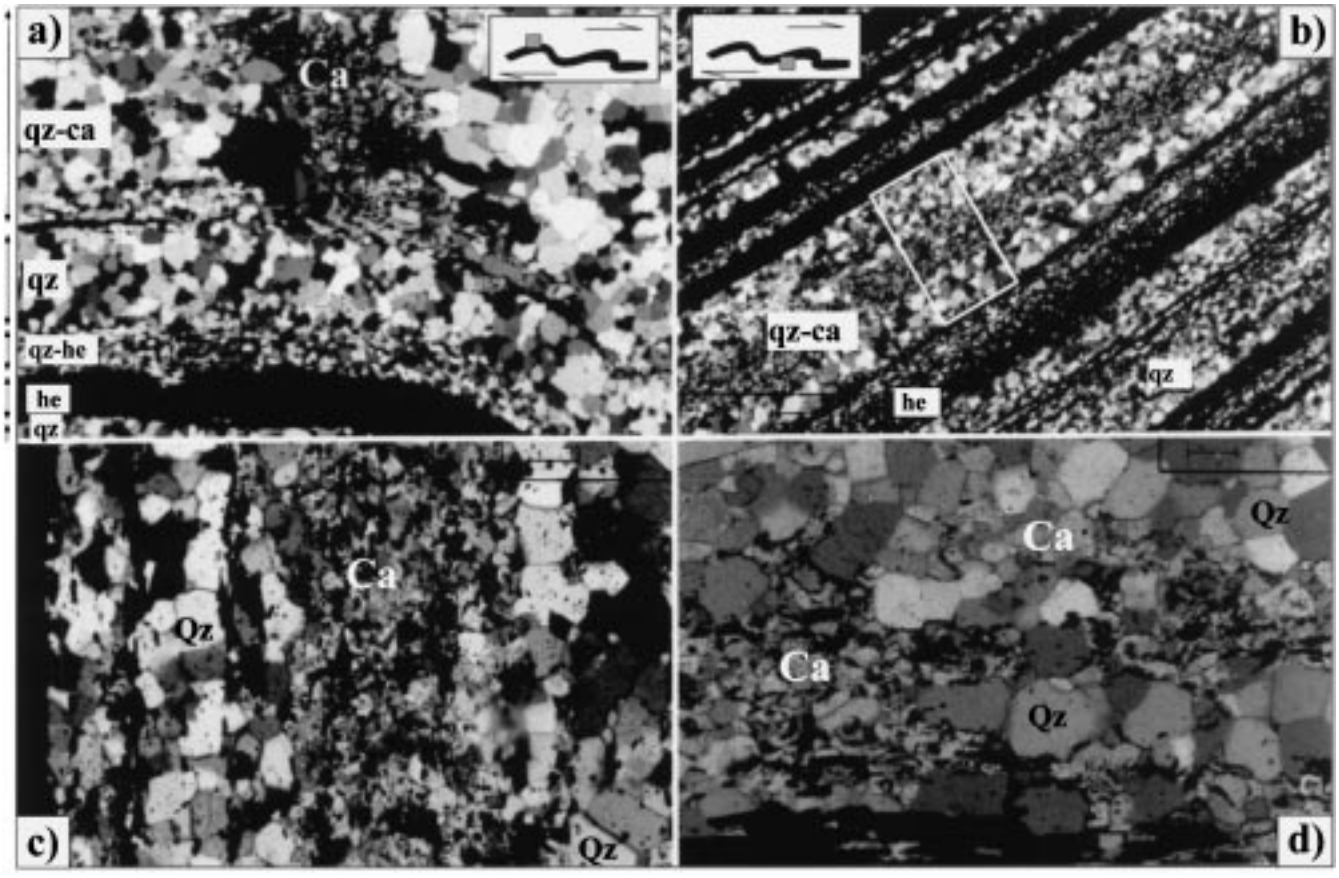

Fig. 4. (a) Photomicrograph showing the four main layer types in the investigated BIF samples: quartz-rich (qz), hematite-rich (he), quartz–calcite (qz–ca) and quartz–hematite (qz–he) layers. The sketch on the right top shows the location of the view relative to the host fold geometry (XPL). Base of photo is 800 μm. (b) Alternating layers in the long limb of a decimetric host fold. A relatively thick quartz–calcite layer (qz–ca) with a clear separation of these two minerals occurs in the centre of the photograph. The boxed area is shown in 'c' (XPL). Base of photo is 2.4 mm. (c) Detail of the quartz–calcite layer showing the mineral separation between quartz (Qz) in the layer margins; and calcite (Ca) in the centre (XPL). Base of photo is 900 μm. (d) Detail of a less differentiated quartz-calcite layer with a more homogeneous distribution of quartz (Qz) and calcite grains (Ca) (XPL). Base of photo is 720 μm.

layers in the hinge zones. These gaps, generally with a half-moon shape, are filled with coarse-grained quartz and are particularly common when the hematite layers are in contact with quartz–calcite layers where separation of these mineral phases took place (Fig. 7; cf. Ramsay, 1967, p. 416). Kinks, crenullation and incipient plane axial foliation also occur in some hinge zones. Hematite layers that are totally disrupted are generally cross-cut by quartz veins.

The quartz–hematite layers (Fig. 4a) are composed of predominant fine-grained polygonal quartz grains (10–30 μm) with a homogeneous distribution of intergranular and intragranular hematite flakes (5–20 μm) which are oriented parallel to the folded surface. These layers, with thickness varying between 50 and 300 μm, are always situated between the hematite-rich and the quartz-rich layers, mostly on the convex side of the folded hematite layers. They are more noticeable in the hinge zones than in the limbs of host folds, and commonly are in opposition with the half-moon gaps, filled with quartz, that occur in the concave side of the folded hematite layers (Fig. 8a). The proportion of these quartz–hematite layers in the whole rock volume increases, as well as the average grain size decreases, with progressive deformation/folding (Fig. 8b).

The quartz-rich layers (thickness 500 μm–30 mm) keep a nearly constant thickness along all the host fold domains and are composed by equigranular polygonal quartz grains (40–90 μm) with minor amounts of hematite and calcite. SEM observation of these grains revealed well-fitted, straight grain boundaries (Fig. 5a) and no apparent intergranular porosity on a scale of a few microns.

3.3. Veins

Three main types of veins occur in the BIF samples relative to their location in the host folds: (1) bedding-parallel veins in the short limbs; (2) axial plane-parallel veins in the hinge zones and (3) cross-cutting veins oriented at high angles to layering in the long limbs of host folds (Fig. 9). All veins are composed predominantly of polygonal aggregates of quartz grains (30–120 μm) with random *c*-axis orientations plus minor amounts of calcite and/or hematite (<3%). Most of these veins are spatially associated with

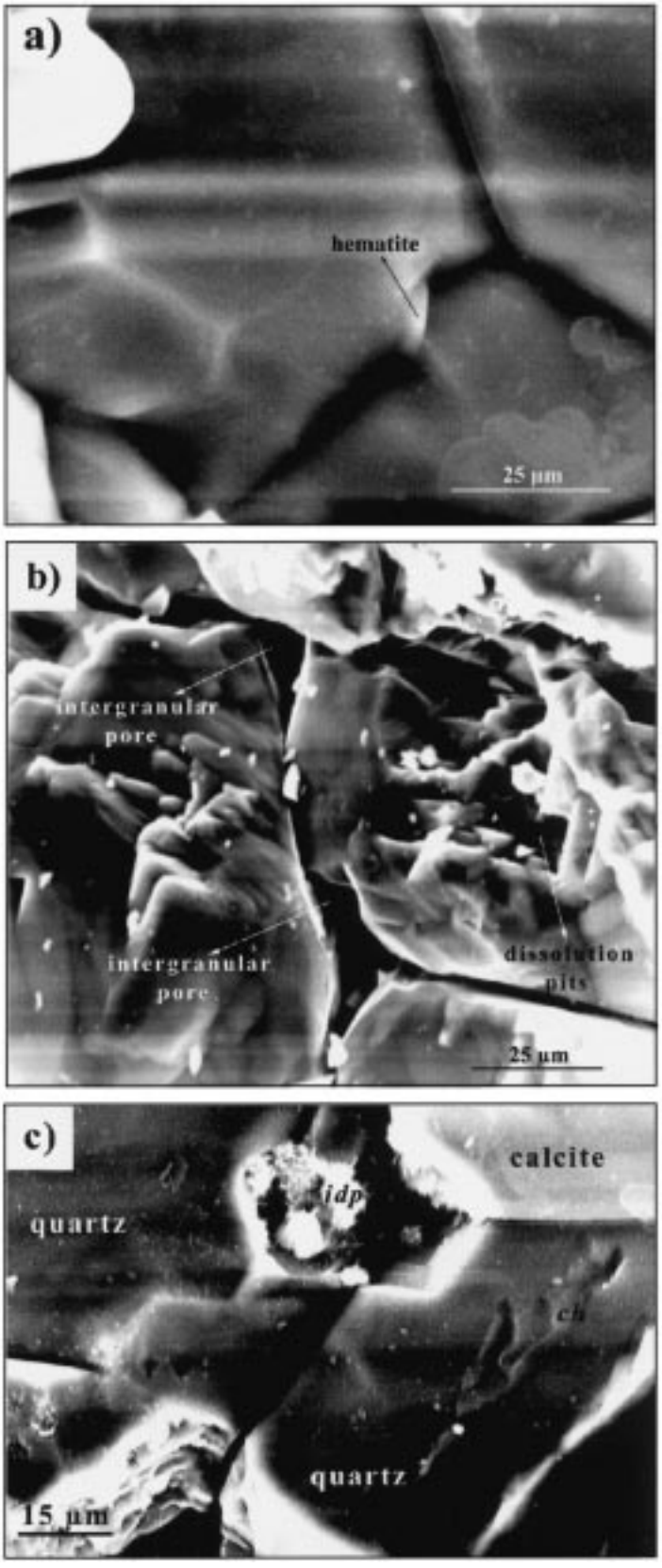
a)
hematite
25 μm
b)
intergranular pore
intergranular pore
dissolution pits
25 μm
c)
calcite
idp
quartz
ch
quartz
15 μm

from quartz–calcite layers where separation of the mineral phases took place.

Bedding-parallel veins occur in the short limbs of the host folds, generally within or immediately adjacent to the thickest hematite layers; many are only one crystal-wide veins. Hematite flakes occur between or inside the quartz grains near the vein margins. Carbonate grains are rare. Axial plane-parallel veins are generally more fine-grained than the others (30–80 μm), and contain only minor amounts of hematite and calcite. These veins appear to have originated from the quartz–calcite layers, exactly in the hinge zones of the host folds, where the adjacent hematite layer is bent or disrupted (Fig. 7). These veins generally cut the thinner layers, but not the thicker ones. Many of these veins terminate in half-moon-shaped gaps formed in the concave side of thicker hematite layers that were not disrupted. The cross-cutting veins in the long limbs of the host folds are oriented at low angles to the inferred maximum shortening direction of finite strain and are formed by coarser-grained quartz and carbonate (60–120 μm) and rare hematite crystals. They also originate from the quartz–calcite layers, but in this case no half-moon gaps occur, as the veins cut most layers, even the thicker ones. Commonly, several narrow veins cluster together to form a thicker, cross-cutting vein.

3.4. c-axis fabrics

Quartz *c*-axis fabrics vary greatly among the different microstructural domains. Both random and preferred *c*-axis orientations are present. Random patterns occur within the polygonal grain aggregates of the quartz–calcite and quartz–hematite layers, whereas moderate to strong fabrics occur in the pure quartz layers (Fig. 10).

The thickest pure quartz layers (>500 μm-thick) show relatively stronger *c*-axis preferred orientation in the form of single-girdle and asymmetric cross-girdle fabric skeletons generally oriented at a high angle to the local shear plane represented by the layer boundaries; this asymmetry being consistent with the overall shear sense inferred from the fold geometry. However, variable patterns are observed among domainal *c*-axis fabrics from different parts of any folded layer. Fig. 11 shows domainal fabrics obtained in a 2 cm-thick pure quartz layer, which was asymmetrically folded. The stronger and most clearly asymmetric fabrics occur in the long limb of the asymmetric fold. In contrast, the short limb shows weaker and poorly characterized *c*-axis fabrics, with a subtle asymmetry relative to the bulk shear that is opposite to that inferred from the overall fold geometry. Random or weak *c*-axis fabrics with an opposing asymmetry relative to the bulk shear occur in the hinge zones.

Totally different fabrics are shown by veins and quartz grains that infill gaps in the hematite layers. Quartz veins show random or very weak preferred orientation of *c*-axes at high angles to the vein walls. Within the gaps opened in the broken hematite layers, the *c*-axes of large quartz grains are generally oriented at high angles to the maximum shortening direction, some at low angles to the inferred gap opening direction (Fig. 10; plot 5), which generally reflects the maximum extension direction of the finite strain ellipsoid. A preferred orientation of *c*-axes at low angle to the bulk shear direction is shown by some thin (<30 μm-thick) one crystal-wide quartz bands. Quartz from the fine-grained quartz–hematite layers (Fig. 10; plots 2 and 4), as well as polygonal quartz and calcite grains from the quartz–calcite layers generally show poorly defined *c*-axis patterns with several scattered submaxima (Fig. 11).

4. Partitioning of deformation processes

4.1. Crystal–plastic deformation

The pure quartz layers accommodate progressive deformation/folding through crystal–plastic processes, as indicated by the typical (although weak) single-girdle and asymmetric type-I cross-girdle fabric skeletons (Lister et al., 1978; Lister and Williams, 1979) present in the fold limbs. The subtle opposing asymmetry of these fabrics relative to the bulk shear plane, when measured in the different fold limbs, is consistent with the expected effect of flexural slip, which may cause opposite shear senses to be recorded in different fold limbs (e.g. Tanner, 1989). In these asymmetric folds, the long limbs generally show more strong *c*-axis fabrics than the short limbs, which is also an expected effect of flexural slip. This is because, in the long limbs of asymmetric folds, the shear component derived from flexural slip is synthetic to the superimposed overall shear. In contrast, in the short limbs, flexural shear and bulk shear are necessarily antithetic. As a consequence, a smaller finite shear strain is recorded in hinge zones and short limbs of folds, as reflected by the presence of weaker *c*-axis fabrics in these domains. Another piece of evidence for operation of flexural slip is the weakening *c*-axis preferred orientation towards the fold hinges, as a consequence of the decreasing shear offset in this direction. The opposing asymmetry of the secondary folds present in the long and short limbs of the host folds is also consistent with this interpretation.

Crystal–plastic deformation and concurrent dynamic

Fig. 5. Scanning electron microscope (SEM) observations of artificially produced intergranular fracture surfaces. (a) Typical well-adjusted grain boundaries of polygonal quartz grains from a quartz rich layer. (b) Porous grain boundaries in quartz grain aggregates from a quartz–calcite layer where separation of the mineral phases occurred. Note the large pores in the grain corners and the irregular ('corroded') shape of the quartz grains. (c) Intergranular porosity in quartz–calcite aggregates, where mineral separation did not occur. Note the intergranular dissolution pit (*idp*) in a quadruple junction between quartz and calcite grains. One 'dissolution channel' (*ch*) is observed on the surface of the quartz grain on the right portion of the photo.

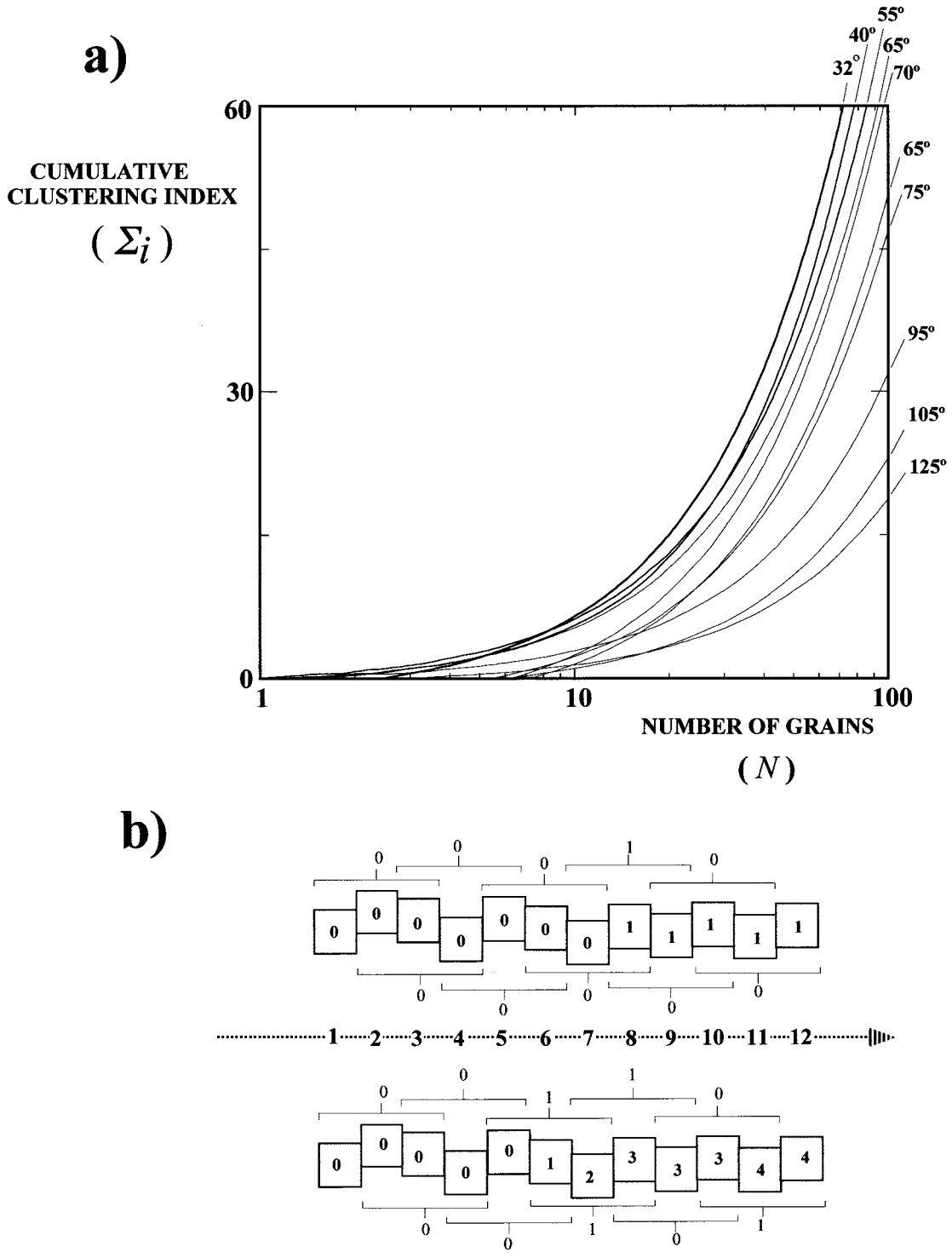

Fig. 6. (a) Diagram showing the results of grain clustering statistics in folded quartz–calcite layers with varied interlimb angles (from 32 to 125°). (b) Sketch illustrating the clustering analysis procedure performed in transversals across the quartz–calcite layers. A clustering index (i) is determined to each group of three grains. If three consecutive grains of the same mineral occur (quartz or calcite), then $i = 1$. If grains of different minerals are adjacent, then $i = 0$. The cumulative clustering index (Si) is determined in each grain along the profile (indicated by the number inside the squares, which represent the individual grains). Note how small changes in the grain distribution can produce significant changes in the clustering pattern.

recrystallization through grain boundary migration (GBM recrystallization; e.g. Urai et al., 1986) can also account well for the sealed grain boundaries of polygonal quartz grains in the pure quartz layers (Fig. 5a). This type of grain boundary microstructure is typically developed in grain aggregates deformed under relatively dry conditions (e.g. Hippertt, 1994b), suggesting that a free fluid phase was not present in these domains during deformation, at least on

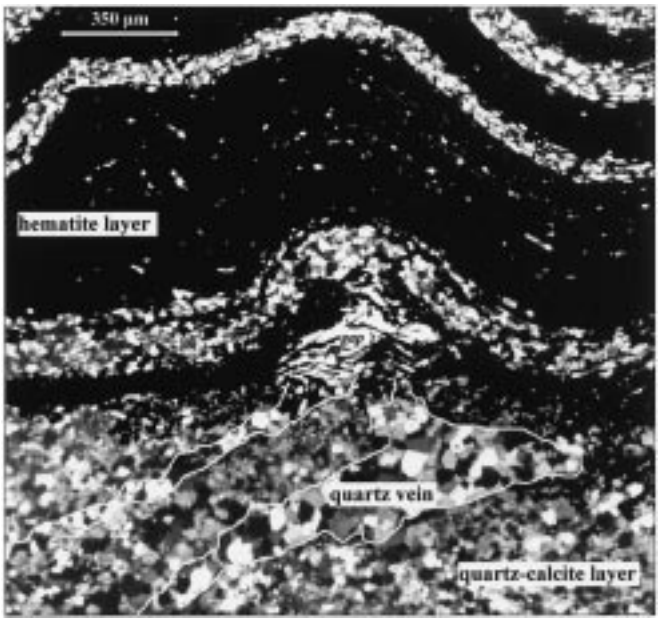

Fig. 7. Photomicrograph showing quartz microveins in the hinge zone of a millimetre-scale secondary fold. Note how the veins originate in the quartz–calcite layer and terminate in the 'half-moon'-shaped gap in the concave side of the bent/disrupted hematite layer (*gap*).

the observed micrometer scale. However, it does not prevent the existence of fluid films, tubes along grain edges, or isolated intergranular fluid pockets on a nanometre scale (e.g. White and White, 1981; Raj, 1982; Spiers and Schutjens, 1990). Nevertheless, deformation conditions in these pure quartz aggregates were comparatively dry relative to other domains, reflecting a heterogeneous fluid access into the multilayered deforming rock.

4.2. Solution transfer creep, brittle deformation, mineral segregation and vein formation

In the quartz–calcite layers, lack of lattice preferred orientation in both quartz and calcite aggregates indicate that intracrystalline slip was not a main deformation process in these layers, and that the development of polygonal aggregates in these domains should be rather attributed to processes such as direct precipitation from a fluid phase (solution-precipitation creep), solid state grow (porphyroblastesis) or readjustment of grain boundaries in initially fine-grained material. In fact, some calcite porphyroblasts which are generally poikiloblastic and much larger than the average grain size do exist in these layers, and appear to have grown over the previously formed polygonal aggregates. Most calcite, however, occurs as polygonal grains in equigranular quartz–calcite aggregates which show a noticeable intergranular porosity (Fig. 5b,c), reflecting the presence of a high volume fluid phase (fluid content $>0.1\%$; cf. Watson and Brenan, 1987) in these domains, at least during the final stages of deformation. This porosity is characterized by the presence of irregular, thermodynamically non-equilibrated pore geometries (e.g. Hippertt, 1994a) which reflect a mobile crystal–fluid interface (i.e. dissolution), suggesting that fluid-assisted solution-precipitation creep was the most likely deformation process for both quartz and calcite in these domains. This porosity is also present in the segregated pure quartz domains (microveins, discussed below), confirming that fluid access was pervasive in the quartz–calcite layers.

One possible explanation for preferential fluid access in these layers is the anisotropic accommodation of plastic strain across the quartz–calcite grain boundaries. In low temperature deformation ($T < 300$°C), calcite is recognized to have lower activation energies for dislocation creep than quartz, apart from being very susceptible to develop deformation twinning in very low grade conditions onwards (Schmid et al., 1981). As a consequence, in these quartz–calcite aggregates, plastic strain of the calcite grains cannot be as efficiently accommodated by the adjacent quartz grains, such that an increasing porosity should form along quartz–calcite grain boundaries. This porosity enables increasing fluid access and reactivity with the crystal aggregates (as indicated by the dissolution features in Fig. 5b,c), enabling solution-precipitation creep to become the dominant deformation process in parallel with the increasing proportion of fluid. Pervasive solution-reprecipitation creep should obliterate any pre-existing microstructures (e.g. deformation twinning) and/or crystallographic fabrics that could have formed during the initial stages of plastic deformation in calcite. This is probably why we do not observe these features in the calcite aggregates. However, some of the disseminated submaxima present in both quartz and calcite fabrics (Fig. 11) might be remnants of earlier lattice preferred orientations produced prior to pervasive solution-reprecipitation creep to take place. On the other hand, such a situation did not occur in the pure quartz layers

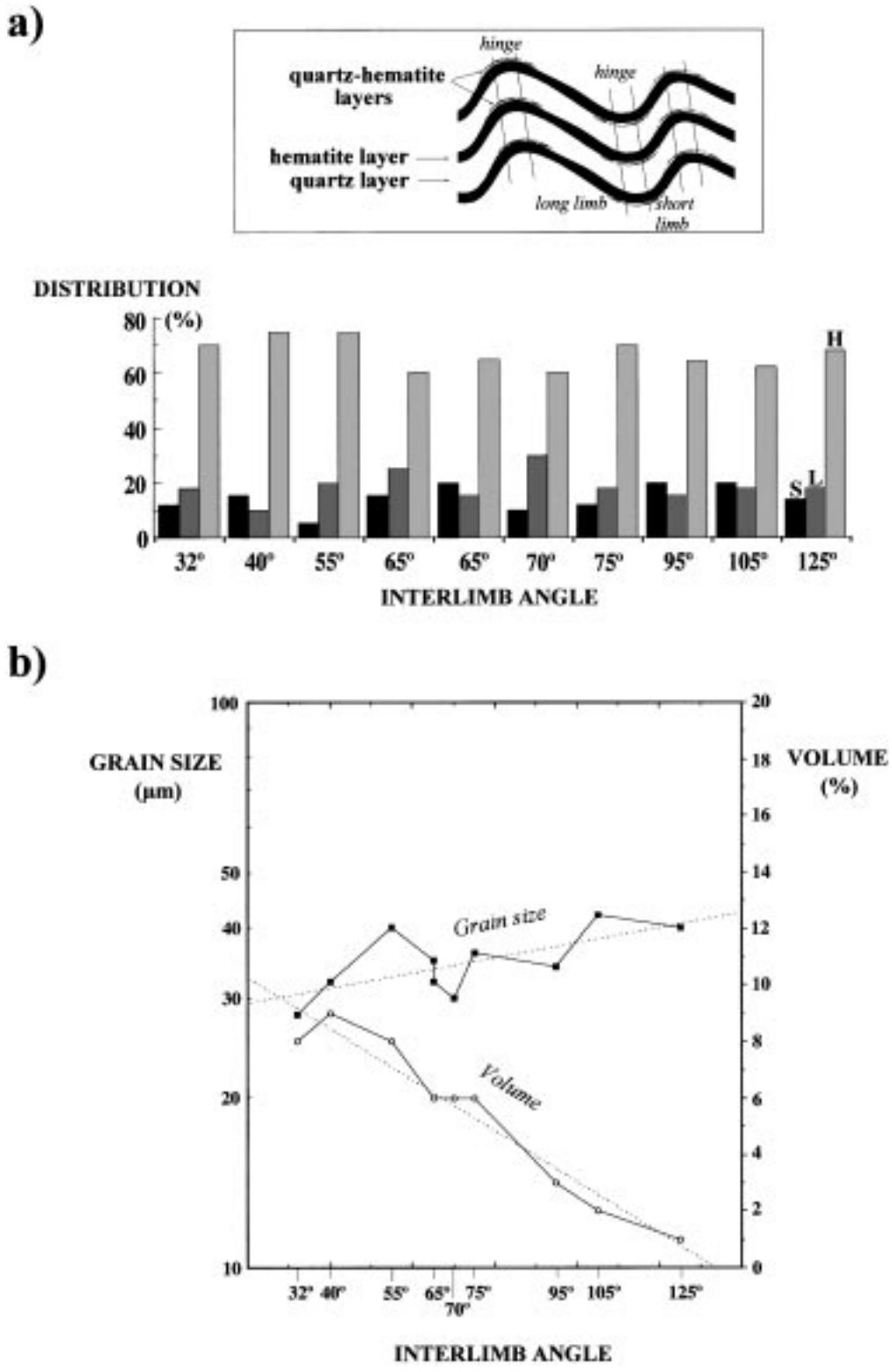

Fig. 8. (a) Histogram showing the distribution of the fine-grained quartz-hematite layers between short limbs (S), long limbs (L) and hinge zones (H) of asymmetric secondary folds. The boxed sketch illustrates the preferred location of these layers in the convex side of folded hematite layers in the hinge zones. (b) Diagram showing the variation of average grain size and volume proportion of the quartz–hematite layers with the progressive fold closure.

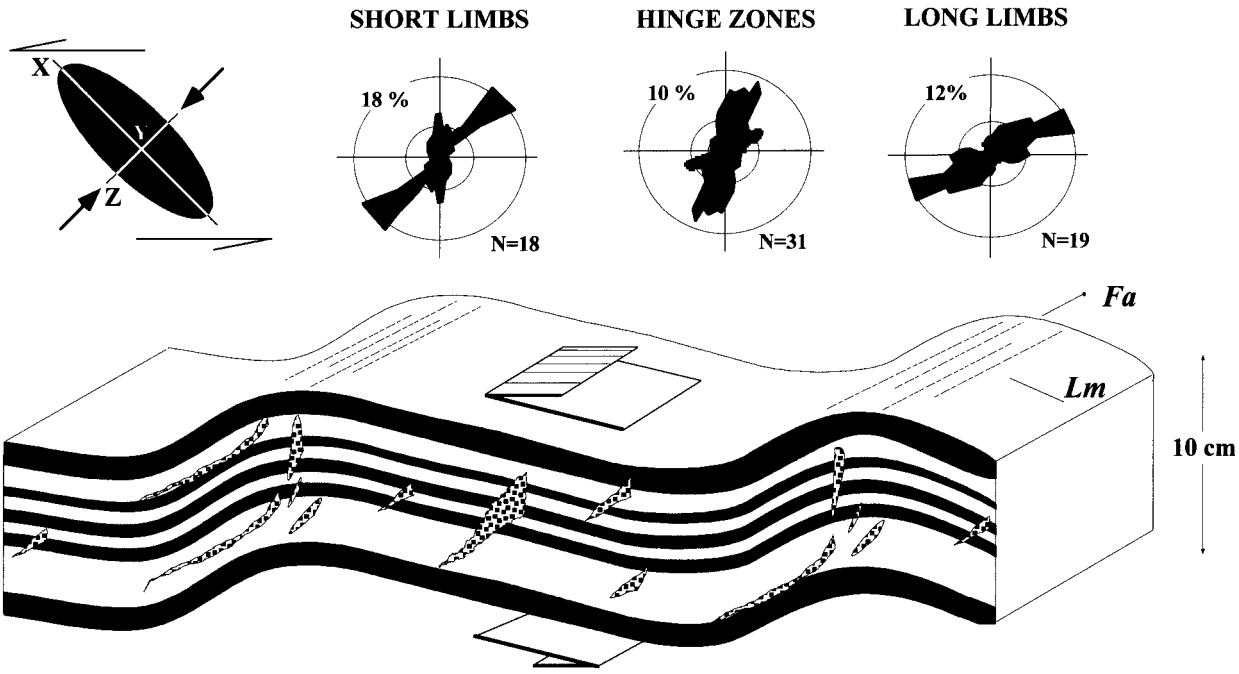

Fig. 9. Sketch with rose diagrams illustrating the orientation of quartz veins in the different domains of the asymmetric, decimetre-scale host folds, as measured in a section perpendicular to the fold axes. The orientation of the local finite strain ellipse, as inferred from grain shape fabrics and plane axial cleavage, is also indicated. Fa and Lm denote orientation of fold axis and mineral lineation, respectively.

where grain boundary migration continuously sealed the quartz–quartz grain boundaries during progressive deformation/dynamic recrystallization, preventing fluid access into the deforming aggregate. This more impermeable microstructure contributed to the continued crystal–plastic deformation in these domains.

Progressive fluid access into the quartz–calcite layers and, as a consequence, pervasiveness of solution transfer processes may explain the observed separation of quartz and calcite in the most strained domains. That is a natural consequence of the different solubilities and ionic mobilities of silica, Ca^{+2}, and $(CO_3)^{-2}$ in aqueous-rich solutions (e.g. Brimhall and Dietrich, 1987; Dipple et al., 1990). An important observation here is that mineral segregation and associated veining in the quartz–calcite layers occur preferentially in domains where fracturing and opening of gaps occurred in the adjacent hematite layers. This suggests that brittle deformation in the hematite layers may also have exerted control on the segregation processes in the adjacent quartz–calcite layers. Indeed, fracturing and opening of relatively large gaps is expected to directly affect the crystal–fluid thermodynamical equilibrium and fluid flow in deforming polymineralic aggregates at low metamorphic grade conditions (Sibson, 1994). This is because the opened gaps act as a sink for the intergranular fluid, and are progressively sealed by direct precipitation of the components that are saturated in the fluid phase (SiO_2 in most crustal ambients; e.g. Selverstone et al., 1991). This precipitation may cause a thermodynamical imbalance in the crystal–fluid system by producing contrasting chemical potentials for silica between fluid phase and crystals, such that quartz or other silicate phases should be dissolved to re-equilibrate the crystal–fluid system (see Shimizu, 1995 for discussion). Indeed, in the focussed quartz–calcite layers, evidence for dissolution is more noticeable in quartz grains than in calcite grains (Fig. 5c), reflecting the higher solubility of silica (around 6 g/kg H_2O at low metamorphic grade conditions; Fournier and Potter, 1982) and a more stable behaviour of calcite. The rate of this process is directly related to the precipitation rate, which in turn depends on the gap opening rate. Therefore, brittle deformation at fast strain rates is expected to favour production of abrupt chemical potential differences between crystal phases and fluid phase, which act as the driving force for pressure solution (Shimizu, 1992).

Pressure solution can also be described as driven by a chemical potential difference between source and sink sites (Paterson, 1995). For the situation considered in this paper (Fig. 12), where quartz infills fractures in hematite, the source spots for silica are the quartz grains in contact with fluid in the quartz–calcite layers. Neglecting surface energy considerations and assuming no elastic/plastic strain in the quartz grains, the chemical potential (μ) of silica in the grain-fluid contacts is given by:

$$\mu \approx \sigma_n V_m \quad (1)$$

where σ_n is the normal stress which varies between σ_1 and σ_3 depending on the grain boundary orientation; and V_m is the molar volume of the solid. Similarly, the chemical potential in the sink sites, i.e. the crystal–fluid interface in

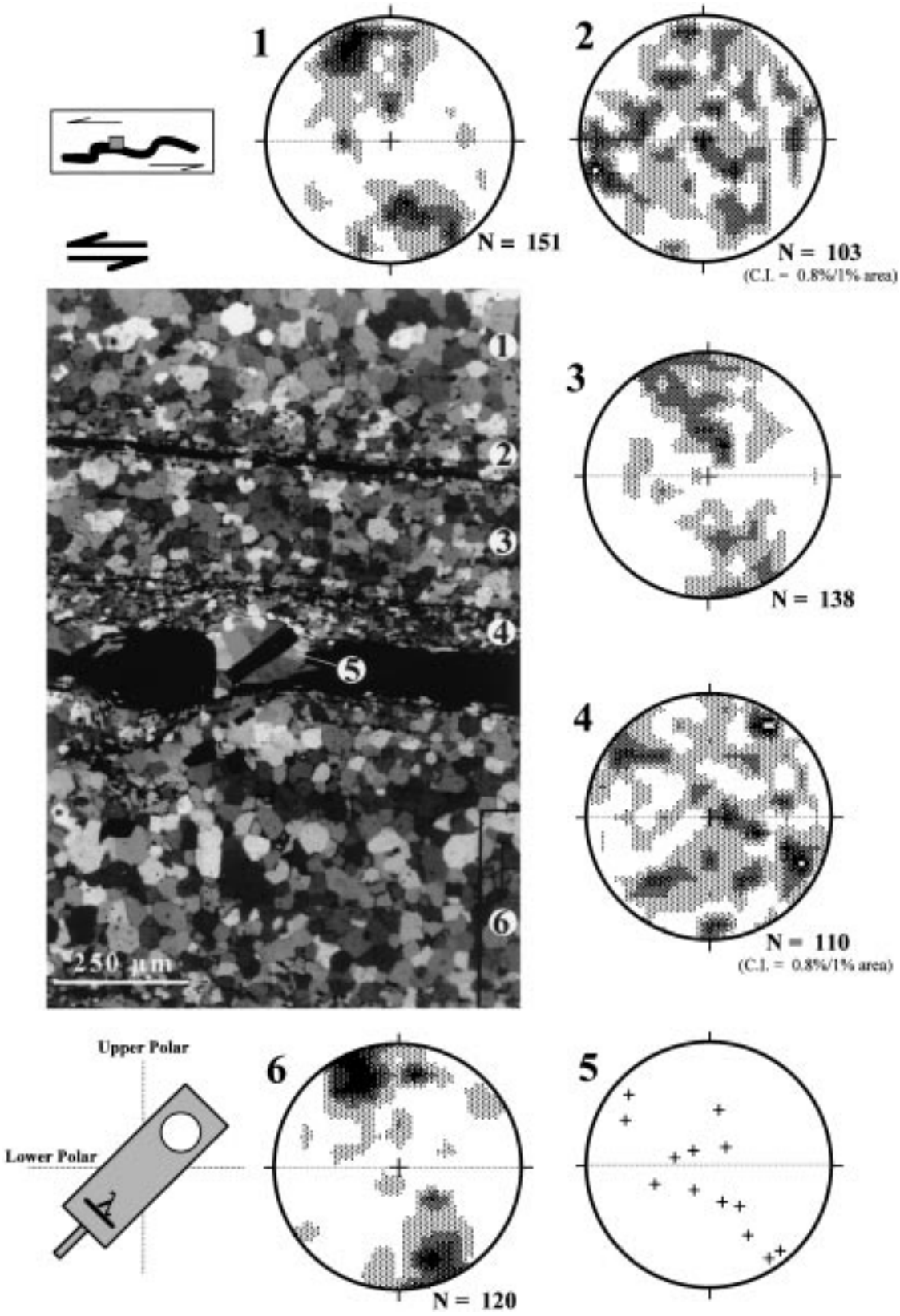

Fig. 10. Domainal *c*-axis fabrics from quartz-rich layers (plots 1, 3, and 6), fine-grained quartz–hematite layers (plots 2 and 4) and elongate quartz grains which fill a gap in the disrupted hematite layer (plot 5), measured on a XZ section. Density contours are 1%1% area, except where indicated different. XPL photomicrograph with the gypsum plate inserted to enphasize the domainal fabrics. Orientation of the gypsum plate, microscope polars and location of the view relative to the host fold geometry are indicated.

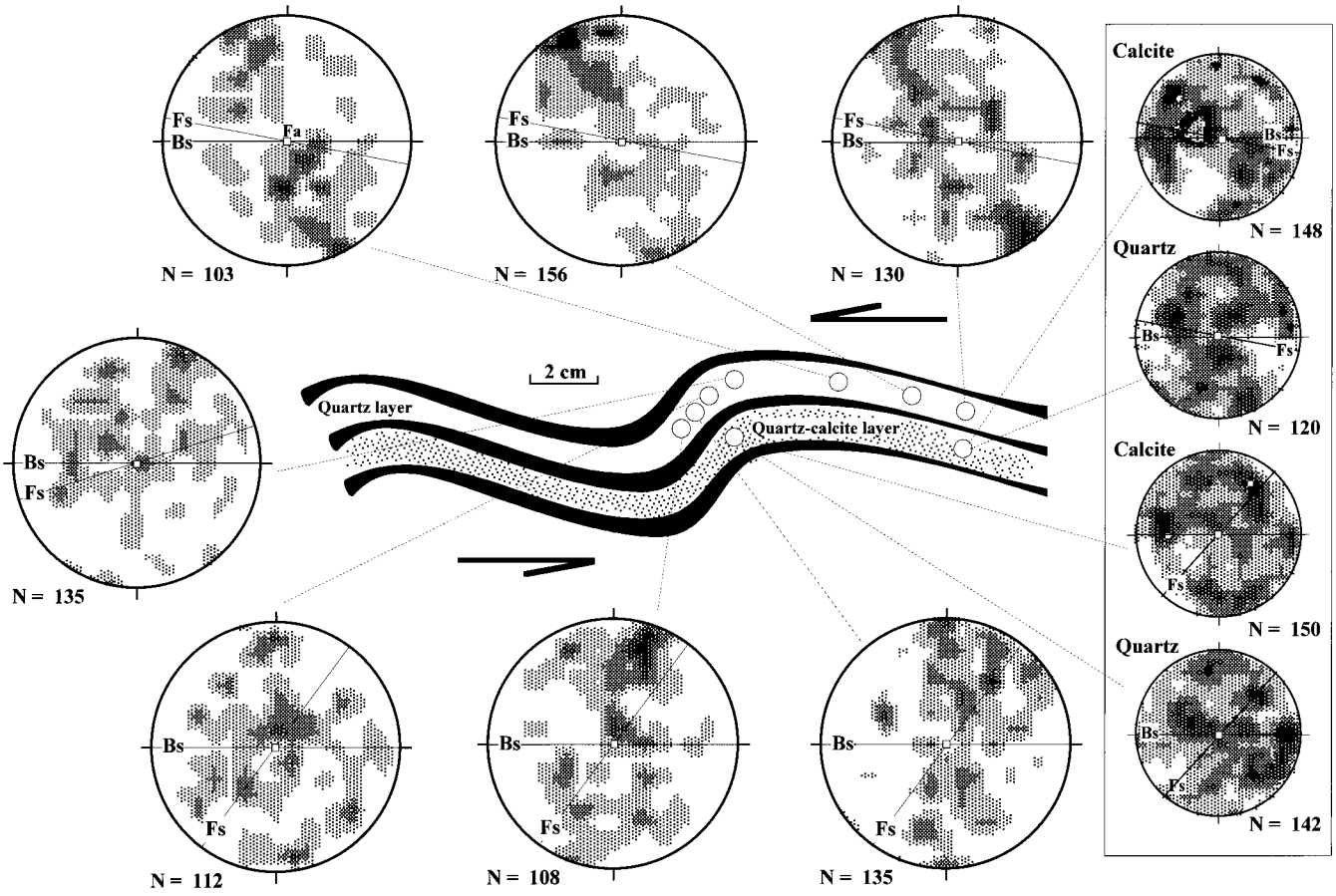

Fig. 11. Domainal *c*-axis fabrics from different domains of folded quartz-rich and quartz–calcite layers, measured on a XZ section. The four boxed plots on the right side of the figure refer to the quartz–calcite layers (Kamb contours, contour interval 1 sigma). The others are from the quartz-rich layer (density contours are 1%/1% area). Fold surface (Fs), fold axis (Fa) and bulk shear plane (Bs) are indicated.

the opened fracture walls, is:

$$\mu \approx p \; V_m \tag{2}$$

where p is the fluid pressure inside the fracture. If no fluid overpressure occurs, and if the fracture wall is oriented parallel to σ_1, p will approach σ_3 when the fracture walls are not moving away. However, in the instant of a separation increment, p will tend to zero and, as a consequence, the largest possible driving potential difference between source and sink sites will be produced, activating solution transfer. This is consistent with the commonly observed coexistence of brittle and solution transfer deformation processes in many low metamorphic grade tectonites (Knipe, 1989) and experimentally deformed rocks (e.g. den Brok, 1992), which can commonly lead to development of typical incremental crack-sealing microstructures (Ramsay, 1980). In summary, we are left with a picture where, by changing the local physical–chemical conditions, operation of a given deformation mechanisms can directly influence other associated deformation processes operating in different domains of the deforming medium.

4.3. Single-layer buckling and granular flow

The quartz–hematite layers show a characteristic microstructure where both quartz and hematite are fine-grained (<20 μm) and quartz shows a random *c*-axis orientation. Flat hematite crystals show a strong shape preferred orientation parallel to the band contacts. All of these characteristics are common in grain aggregates deformed by granular flow (e.g. Stünitz and FitzGerald, 1993) where grain boundary sliding was the main deformation mechanism. The presence of straight, well-fitted polygonal boundaries in all grains, however, suggests that some grain boundary adjustment through grain boundary migration (GBM) or solution-transfer (Paterson, 1995) has also occurred. Granular flow is a common deformation process in low metamorphic grade, fine-grained tectonites from high strain shear zones (e.g. Stünitz and FitzGerald, 1993), as a result of both stress and strain localization. In the investigated folds, we would not necessarily expect granular flow to operate because of the small finite strain recorded in this material. However, the contact between pure hematite and pure quartz layers is a well-marked rheological interface that

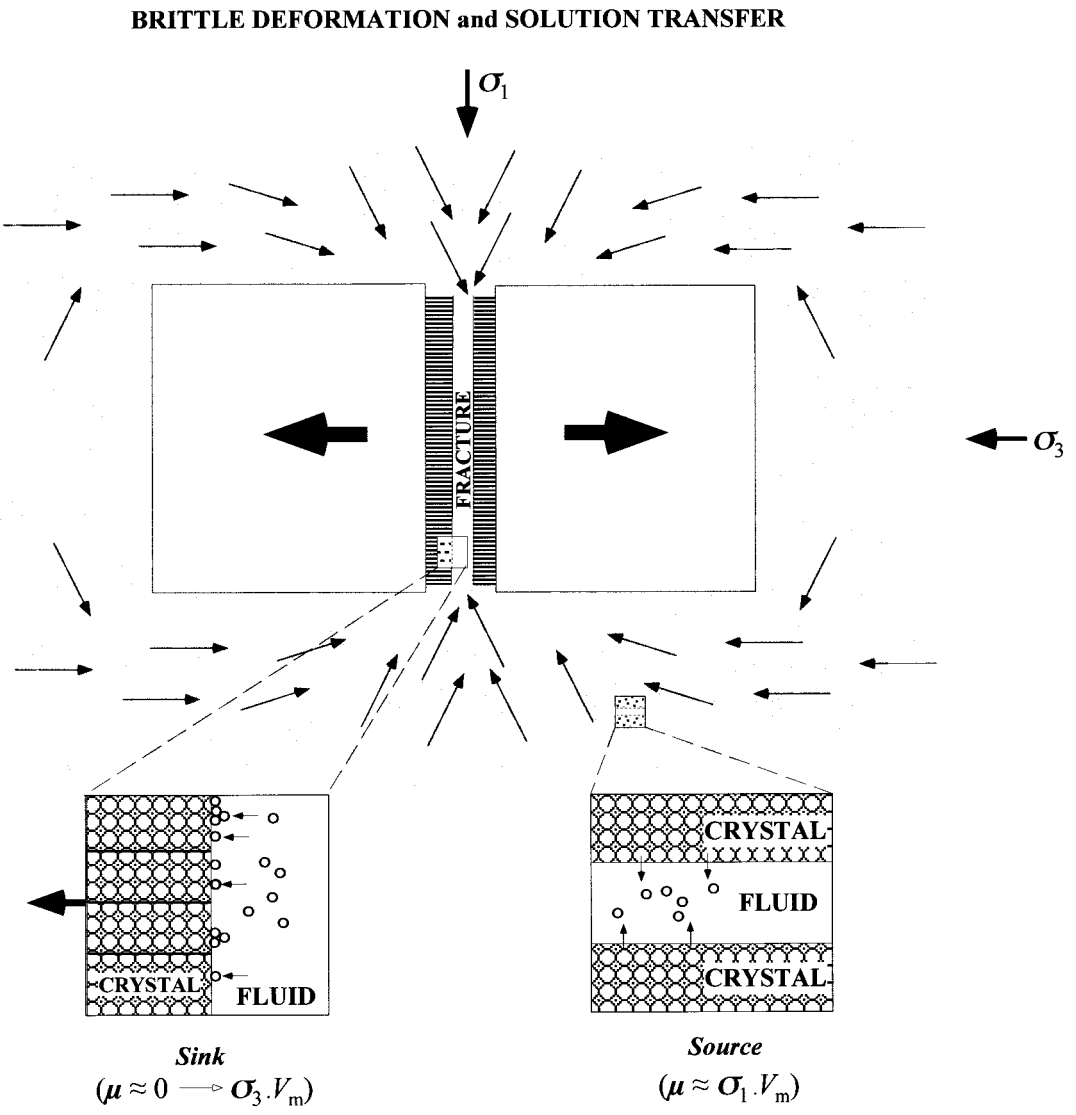

Fig. 12. Sketch illustrating transfer of silica from the matrix quartz grains towards an opening fracture in hematite through the intergranular fluid. If the fracture is oriented parallel to σ_1, the chemical potential (μ) in the fracture walls (sink sites) varies from 0, in the instant of a separation increment, to $\sigma_3 V_m$, when the movement stops. Similarly, the chemical potential in the matrix grain boundaries (source sites) varies between $\sigma_3 V_m$ and $\sigma_1 V_m$ depending on the grain boundary orientation. The maximum driving potential gradient for solution transfer between source and sink domains is produced during the instantaneous brittle deformation increments.

separates two domains deforming by different processes (brittle deformation in hematite; crystal–plasticity in quartz), where stress and strain localization is likely to occur. This causes progressive grain size reduction (by fracturing or dynamic recrystallization) in these domains up to a critical grain size where granular flow become a more economic process. This local granular flow affects both the hematite layers and the quartz layers along the contact, and should destroy any existing crystallographic preferred orientation (e.g. Hippertt, 1998). The increasing presence of these fine-grained quartz–hematite layers in concert with the progressive fold closure argues for their tectonic origin (Fig. 8). One interesting fact is the preferred development of these fine-grained, bi-mineralic layers in the hinge zone of folds, and not in the limbs as it would expected to occur by effect of interlayer flexural shear. We suggest that this distribution resulted from the single layer buckling of some hematite layers, which are constrained between two more plastic quartzose layers. This model is consistent with opening of half-moon-shaped gaps in the concave side of hinge zones, and grain-size reduction in the stretched, convex side. Indeed, these fine-grained layers are particularly more common in the convex side of hinge zones of some relatively thicker hematite layers which were preferentially buckled, as disruption did not occur. This scenario provides another example of coupled deformation deformation processes acting simultaneously in different microstructural domains of the deforming rock, i.e. buckling of hematite layers plus associated grain size reduction and granular flow in the convex contact with the adjacent quartz layers.

5. Conclusions

By investigating folded multilayered rocks from the Quadrilátero Ferrífero granite–greenstone terrain, an attempt was made to show how deformation at low metamorphic grade can be partitioned into a number of plastic, brittle and fluid-assisted deformation mechanisms which are intimately linked and can influence each other. During folding of BIF, quartz deformed by crystal-plasticity, solution transfer or granular flow depending on the characteristics of the grain aggregate and orientation relative to the stress-strain framework. Polymineralic rocks deforming at low metamorphic grade are particularly susceptible to opening of pore space due to anisotropic strain accommodation among grains. This enhances fluid access that may drastically influence the operative deformation mechanisms, with increasing participation of solution transfer processes.

Mineral segregation and quartz veining within the hinge zones by solution transfer appears as an efficient mechanism to promote mass transfer from limbs to hinge zones during folding at low metamorphic grade conditions. The moderate stage of folding in the investigated samples do not permit inferences on the deformation partitioning at higher strain. However, the increasing proportion of this tectonically derived, fine-grained quartz–hematite layers during progressive folding is suggested to reflect the change towards a more homogeneous microstructure where only a few, most economic deformation mechanisms become dominant, as commonly occurs in high strain tectonites such as ultramylonites and phyllonites, where granular flow is common.

Acknowledgements

Financial support for this research was provided by a research grant from the Brazilian National Research Council (CNPq, process 198278-95).

References

Brimhall, G., Dietrich, W., 1987. Constitutive mass balance relations between chemical composition, volume, density, porosity and strain in metasomatic hydrochemical systems. Geochimica et Cosmochimica Acta 51, 567–587.

Castro, L, 1994. Genesis of BIF. Economic Geology 89, 1384–1397.

Chauvet, A., Faure, M., Dossin, I., Charvet, J., 1994. A three-stage structural evolution of the Quadrilátero Ferrífero: consequences for the Neoproterozoic age and the formation of gold concentrations of the Ouro Preto area, Minas Gerais, Brazil. Precambrian Research 68, 139–167.

Chemale Jr, F., Rosière, C.A., Endo, I., 1994. The tectonic evolution of the Quadrilátero Ferrífero, Minas Gerais. Precambrian Research 65, 25–54.

den Brok, B., 1992. An experimental investigation into the effect of water on flow of quartzite. Geologica Ultraectina 95, 1–178.

Dipple, G., Wintsch, R., Andrews, M., 1990. Identification of the scales of differential element mobility in a ductile fault zone. Journal of Metamorphic Geology 6, 645–661.

FitzGerald, J., Stünitz, H., 1993. Deformation of granitoids at low metamorphic grade. I: Reactions and grain size reduction. Tectonophysics 221, 299–324.

Fournier, R., Potter, R., 1982. An equation correlating the solubility of quartz in water from 25 to 900°C at pressures up to 10,000 bars. Geochimica et Cosmochimica Acta 46, 1969–1973.

Handy, M., 1990. The solid state flow of polymineralic rocks. Journal of Geophysical Research 95, 8647–8661.

Herz, N., 1978. Metamorphic rocks of the Quadrilátero Ferrífero, Minas Gerais, Brazil. U.S. Geological Survey, Prof. Pap. 641, C1-C81.

Hippertt, J., 1994a. Microstructures and c-axis fabrics indicative of quartz dissolution in sheared quartzites and phyllonites. Tectonophysics 229, 141–163.

Hippertt, J., 1994b. Grain boundary microstructures in micaceous quartzites: Significance for fluid movement and deformation processes in low metamorphic grade shear zones. Journal of Geology 102, 331–348.

Hippertt, J., 1998. Breakdown of feldspar, volume gain and lateral mass transfer during mylonitization of granitoid in a low metamorphic grade shear zone. Journal of Structural Geology 20, 175–193.

Hippertt, J., Davis, B., 2000. Dome emplacement and syncline development in a granite-greenstone terrain (Quadrilátero Ferrífero, southeastern Brazil). Precambrian Research 102, 99–121.

Hippertt, J., Hongn, F., 1998. Deformation mechanisms in the mylonite-ultramylonite transition. Journal of Structural Geology 20, 435–1448.

Knipe, R., 1989. Deformation mechanisms-recognition from natural tectonites. Journal of Structural Geology 11, 127–146.

Lister, G., Paterson, M., Hobbs, B., 1978. The simulation of fabric development in plastic deformation and its application to quartzite: the model. Tectonophysics 45, 107–158.

Lister, G., Williams, P., 1979. Fabric development in shear zones: theoretical controls and observed phenomena. Journal of Structural Geology 1, 283–297.

Marshak, S., Alkmin, F., Jordt-Evangelista, H., 1992. Proterozoic crustal extension and the generation of dome-and-keel structure in an Archaean granite-greenstone terrane. Nature 357, 491–493.

Paterson, M., 1995. A theory for granular flow accommodated by material transfer via an intergranular fluid. Tectonophysics 245, 135–152.

Raj, R., 1982. Creep in polycrystalline aggregates by matter transport through a liquid phase. Journal of Geophysical Research 87, 4731–4739.

Ramsay, J., 1967. Folding and Fracturing of Rocks. McGraw-Hill, p. 562.

Ramsay, J., 1980. The crack-seal mechanism of rock deformation. Nature 284, 135–139.

Schmid, S., Casey, M., Starkey, J., 1981. The microfabric of calcite tectonites from the Helvetic nappes (Swiss Alps). In: McClay, K., Price, N. (Eds.). Thrust and nappe tectonics, Special Publication of the Geological Society of London 9, pp. 151–158.

Selverstone, J., Morteani, G., Staude, J.-M., 1991. Fluid channelling during ductile shearing: transformation of granodiorite into aluminous schist in Tauern Window, Eastern Alps. Journal of Metamorphic Geology 9, 419–431.

Shimizu, I., 1992. Nonhydrostatic and nonequilibrium thermodynamics of deformable materials. Journal of Geophysical Research 97, 4587–4597.

Shimizu, I., 1995. Kinetics of pressure solution creep in quartz: theoretical considerations. Tectonophysics 245, 121–134.

Sibson, R., 1994. Crustal stress, faulting and fluid flow. In: Parnell, J. (Ed.). Geofluids: Origin, Migration and Evolution of Fluids in Sedimentary basins, Geological Society of London Special Publication 78.

Spiers, C., Schutjens, P., 1990. Densification of crystalline aggregates by fluid phase diffusion creep. In: Barber, D., Meredith, P. (Eds.). Deformation Processes in Minerals, Ceramics and Rocks. Unwin Hyman, London, pp. 334–353.

Stünitz, H., FitzGerald, J., 1993. Deformation of granitoids at low metamorphic grade. II: Granular flow in albite-rich mylonites. Tectonophysics 221, 269–297.

Tanner, P., 1989. The flexural slip mechanism. Journal of Structural Geology 11, 635–655.

Urai, J., Means, W., Lister, G., 1986. Dynamic recrystallization of minerals.

In: Hobbs, B., Heard, H. (Eds.). Mineral and Rock Deformation: Laboratory Studies. American Geophysical Union, Geophysical Monograph 36, pp. 61–99.

Watson, E., Brenan, J., 1987. Fluids in the lithosphere, 1. Experimentally determined wetting characteristics of CO2-H2O fluids and their implications for fluid transport, host-rock physical properties and fluid inclusion formation. Earth and Planetary Sciences Letters 85, 497–515.

White, J., White, S., 1981. On the structure of grain boundary in tectonites. Tectonophysics 78, 613–628.